Journal of
Mechanical
Science and
Technology

Journal of Mechanical Science and Technology 21 (2007) 1964~1972

Multidimensional visualization and clustering for multiobjective optimization of artificial satellite heat pipe design

Min-Joong Jeong[1,*], Takashi Kobayashi[2] and Shinobu Yoshimura[3]

[1]*e-Science Applications Research Team, Korea Institute of Science and Technology Information, Daejeon, Republic of Korea*
[2]*Design Systems Engineering Center, Mitsubishi Electric Corportion, Japan*
[3]*Institute of Environmental Studies, The University of Tokyo, Japan*

(Manuscript Received August 17, 2006; Revised July 5, 2007; Accepted July 5, 2007)

Abstract

This study presents a newly developed approach for visualization of Pareto and quasi-Pareto solutions of a multiobjective design problem for the heat piping system in an artificial satellite. Given conflicting objective functions, multiobjective optimization requires both a search algorithm to find optimal solutions and a decision-making process for finalizing a design solution. This type of multiobjective optimization problem may easily induce equally optimized multple solutions such as Pareto solutions, quasi-Pareto solutions, and feasible solutions. Here, a multidimensional visualization and clustering technique is used for visualization of Pareto solutions. The proposed approach can support engineering decisions in the design of the heat piping system in artificial satellites. Design considerations for heat piping system need to simultaneously satisfy dual conditions such as thermal robustness and overall limitation of the total weight of the system. The proposed visualization and clustering technique can be a valuable design tool for the heat piping system, in which reliable decision-making has been frequently hindered by the conflicting nature of objective functions in conventional approaches.

Keywords: Multidimensional visualization; Clustering; Multiobjective optimization; Heat pipe design; Artificial satellite

1. Introduction

When considering the enormous launch expenses and maintenance costs, designers must satisfy strict design criteria, such as performance, reliability, weight, flexibility, and the structural integrity, for most of the components of an artificial satellite. Thus, satisfying the above criteria naturally poses a multiobjective optimization problem that has innumerable alternative solutions, also known as Pareto solutions. With no unique and/or superior design solution, designers have had difficulty in making unanimously acceptable decisions on a single design out of the numerous Pareto solutions. Two different approaches are commonly used to overcome the difficulties in the decision-making (DM) process for a multiobjective optimization problem. First, the preference method literally assigns fixed weights on preferences with respect to each design objective before initiating the optimization to find a unique design solution for DM. Second is the trade-off method, which is used to make a decision from the Pareto solutions after optimization. However, attempts for DM using the preference or trade-off method easily yield poor design outcomes, mainly because a single solution can be inadequate or even unrealistic if the designer needs to satisfy other criteria, such as durability and/or manufacturability, in the overall design [1,2]. Therefore, designers should be provided with a set of Pareto solutions along with supporting knowledge of the solutions so that they can judiciously use the information to choose a better design alternative. Multidimensional visualization has been one of the most supportive tools in guiding feasibility and correlation among

*Corresponding author. Tel.: +82 42 869 0632, Fax.: +82 42 869 0789
E-mail address: jeong@kisti.re.kr

design parameters, objective functions, and practical considerations in the conceptual design stage [3,4]. However, Pareto solutions inherently belong to the outcomes of a multidimensional problem, hindering solid DM for a unique design.

This paper proposes a synchronous 3-dimensional visualization technique that illustratively interprets Pareto solutions of a multiobjective optimization problem. The advantages of this technique will be demonstrated through an example of a practical application of a heat pipe system design in an artificial satellite [5]. Two different objective functions and five independent design parameters were considered in determining the dimension of the physical shape of the heat pipe and maximizing its performance. The multidimensional parameters and function spaces are divided into several lower-order dimensional spaces such as two or three dimensional plots. Each set of data corresponding to a line segment in the lower dimensional plots not only provides feasible solution sets for designers but also helps them to visualize the physical shape of the real design. Therefore, the designer can conceptually understand the correlation of design parameters among the optimized solutions. Furthermore, this study introduces a clustering approach, which considers a set of Pareto solutions as a group of several distinctive clusters. The approach consists of clustering the solutions according to their functional characteristics and design parameters. The Euclidean distance and a point symmetry distance have been used to measure the similarity and dissimilarity of the solutions. With the proposed approach, we can search for the information that supports engineering decision for the design of artificial satellite heat pipe.

2. Multiobjective optimization of artificial satellite heat pipe

In general, a cooling system in artificial satellites consists of heat pipes that are embedded on isothermal radiator panels. The fin efficiency, representing the performance of the cooling system, can be dramatically improved by employing the matrix layout of orthogonally interconnected heat pipes, as shown in Fig. 1. To maximize the fin efficiency of isothermal panels, minimizing the temperature gradient between the lateral and header heat pipes becomes a crucial design objective [8]. On the other hand, reducing the total weight of the thermal control subsystem is also important to minimize the payload on the booster-rocket. A satellite panel is embedded with many aluminum heat pipes, which generally occupy over 50% of the total mass of the radiator panels. Thus, the design of a thermal system in an artificial satellite requires both high fin-efficiency and mininal weight of the heat pipes. Additionally, the operating temperature of the heat widely ranges from $-20.0^{\circ}C$ to $60.0^{\circ}C$ in orbit. The thermal performance of the heat pipes must remain stable and predictable even under an abrupt variation of the outside temperature. Therefore, the temperature dependency of the pipes must be also considered in the heat pipe design. In this study, at first, a combination of Response Surface Methodology (RSM) and Monte Carlo simulation was applied to formulate the mass and thermal functions of the pipe structure [9,10]. Here, design variables were the parameters that defined the shapes of the heat pipes in the satellite panel, while the total weight and thermal robustness of heat pipes became the objective functions.

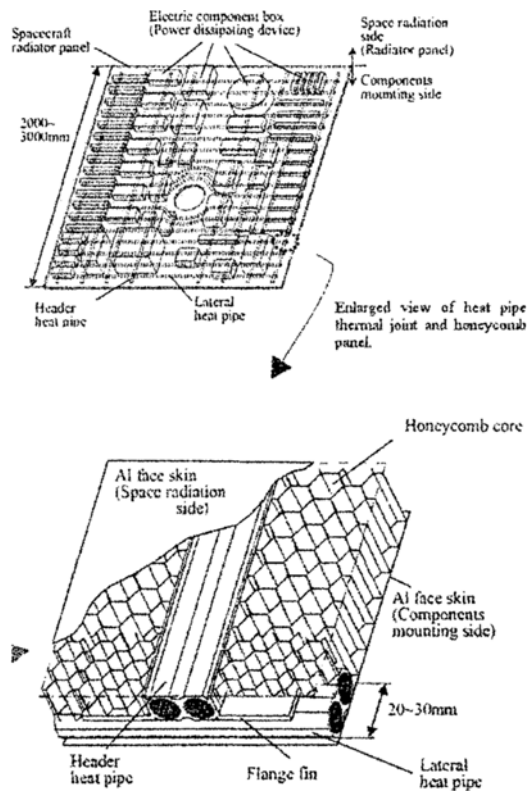

Fig. 1. Layout of heat pipes for satellite radiator [5].

Heat pipe designers must determine the following design parameters: (i) length of fin (L_f), (ii) cutting length of adhesive attached area (L_c), and (iii) thickness of fin (t_f) as illustrated in Fig. 2. The allowable ranges of the design parameters are given in Table 1. Note, that (iv) adhesive thickness (t_b) and (v) operation temperature (T_{op}) are parameters that cannot be controlled by heat pipe designers but significantly affect the thermal performance of the heat pipes. The lateral and header heat pipes are bonded together at the flange fin area with conductive epoxy. The adhesive thickness, t_b has manufacturing tolerance, which influences the thermal performance of the heat pipes. To include this tolerance factor, the adhesive thickness was randomly assigned to values between 0.12mm and 0.22mm having statistics of normal distribution. For normal operation of the satellite, the operating temperature (T_{op}) for heat pipes had to be in the range of $-20.0°C$ through $60.0°C$. Besides,

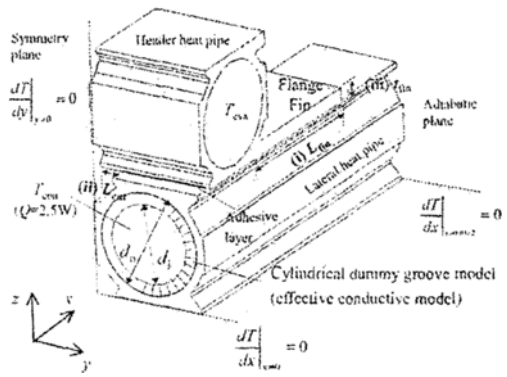

Fig. 2. Design parameters in 3D FE analysis model of heat pipes [5].

Table 1. Design parameter bounds.

Prameter	Lower Bound	Upper Bound
L_f	10.0mm	25.4mm
L_c	1.5mm	2.5mm
t_f	1.0mm	1.7mm

Table 2. Uncertain design parameters.

Parmeter	t_b	T_{op}
Lower Bound	0.12mm	$-20.0°C$
Upper Bound	0.22mm	$60.0°C$
Probability Distribution	Normal Distribution μ=0.17, σ=0.016	Normal Distribution μ=20.0, σ=14.3

the temperature dependency of the heat transfer coefficientsof the evaporator and condenser at the inner wall of an individual heat pipe cannot be neglected if the stability of the thermal system is to be considered. Consequently, uncertain or uncontrollable design variables such as t_b and T_{op} were considered as robust design parameters. Their ranges of variation are described in Table 2. Three levels of experimental design for five design parameters produced 27 analysis points [9~11,20]. Those points were used to select the combination of the analysis parameters that could minimize the total number of finite element analyses.

2.1 Generation of fitted estimation equations

Twenty-seven finite element analyses were performed to calculate the thermal performance of the heat pipes of parametric combinations, which were obtained from the Taguchi orthogonal array-L27 [9,11]. These performance results were used to construct the equation for estimating the characteristic values of the thermal conductance (G) and the total mass (M). Chebyshev's equation was considered to correlate the regression coefficients in multiple linear regression models. The calculated value G that indicates the thermal conductance across the thermal joints in heat pipes is defined as:

$$G = \frac{Q}{T_{con} - T_{eva}} \tag{1}$$

where T_{con} is the condensed liquid temperature in the lateral heat pipe and T_{eva} is the vapor temperature in the header heat pipe. Also, Q is the assumed quantity for the transported heat of 2.5W per thermal joint. The determined response surface equation of G is denoted as $\hat{G}$:

$$\begin{aligned}\hat{G} = f(L_f, L_c, t_f, t_b, T_{op}) &= 0.3745378 - 0.9352909t_b \\ &+ 1.01612t_b^2 + 2.324128e^{-2}L_c - 7.209993e^{-3}L_c^2 \\ &+ 1.838379e^{-3}L_f - 5.379707e^{-5}L_f^2 + 2.447391e^{-2}t_f \\ &+ 2.304583e^{-3}t_f^2 - 6.483411e^{-4}T_{op} - 9.232971e^{-7}T_{op}^2 \\ &- 2.259702e^{-2}t_bL_c - 4.735652e^{-3}t_bL_c^2 + 0.1102442t_b^2L_c \\ &- 9.702533e^{-3}t_b^2L_c^2 + 5.382211e^{-3}t_bL_f - 9.540484e^{-5}t_bL_f^2 \\ &+ 5.15048e^{-3}t_b^2L_f - 1.232524e^{-4}t_b^2L_f^2 + 0.2972589t_bt_f \\ &- 0.1052935t_bt_f^2 - 0.5422262t_b^2t_f - 0.1829687t_b^2t_f^2\end{aligned} \tag{2}$$

Likewise, the response surface equation for the total mass, $\hat{M}$, is also expressed by the following equation:

$$\hat{M} = f(L_f, L_c, t_f, t_b) = (1313.877 - 75.5L_c + 11.0L_c^2 + 1.402597L_f - 1.278314e^{-15}L_f^2 + 62.38776t_f - 6.122449t_f^2 - 380.8t_b + 1120t_b^2) \times 21 \quad (3)$$

3. Multidimensional pareto solutions and synchronous visualization

Pareto solutions of Eqs. (2) and (3) were searched by using the Intermediate Tendency (IT) optimizer [12,13]. The optimizer can be characterized as a type of genetic algorithm, having typical genetic operators such as fitness evaluation, selection, and mutation. To improve the searching efficiency, the optimizer adopts IT recombination, which is more robust than other conventional intermediate recombinations in searching speed. In conventional recombination, such as the global intermediate recombination, any offspring individual cannot jump out from d-dimensional search space covered by their parental individuals. In other words, if an optimum point is located out of the search space, no offspring can reach the optimum point by recombination process alone. The IT recombination, however, yields offsprings depending on the level of discrepancy between parental individuals and randomly selected ones. The degree of discrepancy is usually referred to as a *tendency* in evolution processes, and the offsprings are generated by adding the tendency to their parents. Therefore, the individuals of subsequent iteration are not bound to their parental search space. The superior performance of the IT recombination is shown in Ref. [12,13]. For multiobjective optimization, the optimizer randomly changes its preferences between two objective functions and searching strategy for Pareto solutions in function space. Fig. 3 shows the Pareto solutions and also quasi-Pareto solutions, which were gathered during the optimization process. The quasi-Pareto solutions are the solutions very close to the Pareto front. As shown in Fig. 3, there are many quasi-Pareto and Pareto solutions. The next section will explain the method for finding engineering information from these solutions.

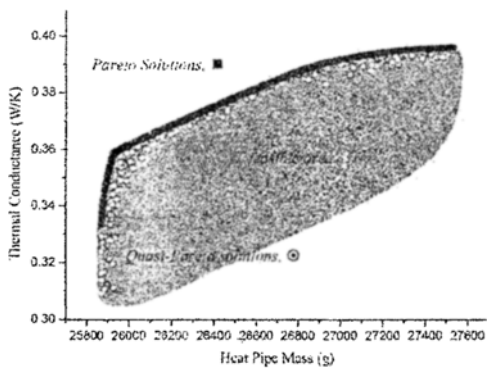

Fig. 3. Pareto solutions and quasi-Pareto solutions in function space.

3.1 Synchronous visualization of functions and parameter spaces

Obtaining meaningful information for finalizing a single solution is not an easy task, especially, if there are many Pareto solutions in multidimensional space. Although parallel-coordinate methods [14,15] can handle multidimensional solutions, the approaches are limited to a certain number of solution sets and their dimensions. To overcome this difficulty, synchronous 3D visualization is proposed. Here, each of the multidimensional parameter and function spaces is subdivided into several 2D or 3D subspaces, and visualized simultaneously. Each solution is visualized in all the subspaces, and the corresponding points in the subspaces are connected by line segments. The real world space is also visualized at the same time. Through the interactive operation of the present visualization system, engineers can explore and understand the correlation among multidimensional function and parameter spaces and the real world space.

During the heat pipe optimization, a 5-dimensional design parameter space was split to 2D and 3D subspaces, i.e., the 2D space of the two uncontrollable parameters and the 3D space of the three shape parameters. Here, the objective functions of 2D space, $\hat{M}$ and $\hat{G}$, were the same, while the two-parameter subspaces and one-function space were visualized simultaneously. Fig. 4 shows the concept of the proposed visualization. The solutions in the original 7D space were divided into the two-parameter spaces and one-function subspace. Moreover, the corresponding physical shape of the heat pipe was visualized along with the subspaces: equivalent design points shown in the different subspaces were connected by line segments. Therefore, it is easy to grasp the physical level of correlation between subspace and solution. The aforementioned visualization system was developed by using the C language and graphic-programming libraries called ADVENTURE AutoGL [16]. A programmable graphical user interface is also provided.

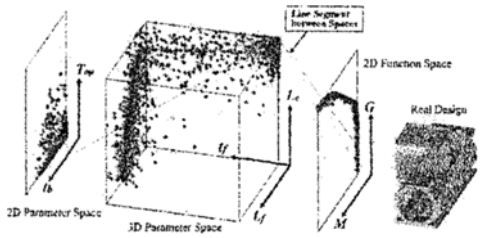

Fig. 4. Synchronous visualization of parameter subspaces, function space and real world design.

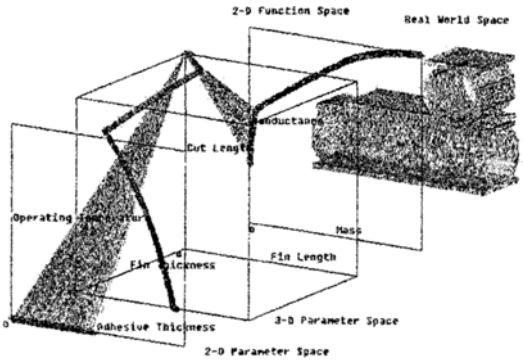

Fig. 5. Synchronous visualization of Pareto solutions of heat pipes.

The quasi-Pareto solutions obtained through iteration are shown in Fig. 4. The figure exhibits a specific position of the design parameters that consititue the optimal values. For example, thin t_b and low T_{op} positively improve the optimum point. However, long L_f with small L_c and t_f will be in conflict with one another. From this visualization, engineers can easily receive ideas on the parametric sensitivity of the current design shape of the heat pipe system. In addition, the set of optimal points in visualization can be considered as Pareto solutions. The effects of t_b and T_{op}, i.e., the mass and conductance, on the objective function space, are assessed in Fig. 5. In the figure, the line segments visualize the correlation between subspaces. As shown in the figure, the operating temperature is at its minimum level, and only the variation of the adhesive thickness causes the changes of the objective functions $\hat{G}$ and $\hat{M}$.

Three different shape parameters, i.e., L_f, L_c and t_f, are almost tied up at the same point in the parameter subspace. Thus, if the shape parameters L_f, L_c and t_f cannot be changed, the apparent design objectives, i.e., minimizing total mass and maximizing heat conductance, can be only achieved by using thinner adhesive (t_b) at a low temperature (T_{op}). However, it is impractical to expect that the operating temperature can be changed. Moreover, controlling the thickness of the adhesive involves a significant amount of uncertainty considering its manufacturing allowance. For enhancing the performance of a heat pipe, therefore, it is important to exploit the correlation of shape parameters and objective functions such that the equations of $\hat{G}$ and $\hat{M}$ are regenerated to incorporate the uncertainties of t_b and T_{op}. In other words, while the equations only include three shape parameters, random values were assigned to t_b and T_{op} according to the probability distributions described in Table 2.

3.2 Estimation equations considering uncertain parameters

The adhesive thickness (t_b) is assigned random values with normal distribution of $\mu_{t_b} = 170.0\mu$ m and $\sigma_{t_b} = 16.7\mu$ m. Likewise, the operating temperatures (T_{op}) have $\mu_{T_{op}} = 20.0°C$ and $\sigma_{T_{op}} = 14.3°C$. A direct sampling of t_b and T_{op} by the Box-Muller method for Monte Carlo simulation is performed to simulate the random 2D parameters of adhesive thickness t_b and operating temperature T_{op}. The number of samples for the Monte Carlo simulation was 1,000,000. To assess thermal robustness, the average value of thermal conductance, $\bar{G}_R$, was defined as follows:

$$\bar{G}_R = \int_{-20}^{60}\int_{0.12}^{0.22} G(t_b, T_{op}) \cdot f_p(t_b, T_{op}) dt_b dT_{op} \tag{4}$$

$$\cong \frac{1}{N}\sum_{m=1}^{1000}\sum_{n=1}^{1000} \hat{G}_R(t_{b,m}, T_{op,n}) \tag{5}$$

where, $f_p(x)$ is the probability density function and N is the total number of samples for the Monte Carlo simulation ($N = m \times n = 1,000,000$). The fitted polynomial equations of $\hat{\bar{G}}_R$ and $\hat{\bar{M}}_R$ are regenerated by using a quadratic model, where the probability density function of the uncontrollable parameters t_b and T_{op} is embedded as

$$\hat{\bar{G}}_R = 2.261369e^{-2}L_c - 8.299937e^{-3}L_c^2 + 2.905449e^{-3}L_f - 7.364545e^{-5}L_f^2 + 5.925684e^{-2}t_f - 1.028177e^{-2}t_f^2 + 0.2312513 \tag{6}$$

$$\hat{\tilde{M}}_R = (1283.375 + 1.402597L_f - 1.278314e^{-15}L_f^2 - 75.5L_c + 11.0L_c^2 + 62.38776t_f - 6.122449t_f^2) \times 21 \quad (7)$$

4. Clustering pareto solutions

Fig. 6 shows Pareto and quasi-Pareto solutions of $\hat{\tilde{G}}_R$ and $\hat{\tilde{M}}_R$. Apparently, Pareto and quasi-Pareto solutions have almost the same function values. However, the quasi-Pareto solutions show larger variance in parameter space than the Pareto solutions. From an engineering standpoint, quasi-Pareto solutions having parametric variance seem better than Pareto solutions because design freedom such as manufacturability is increased. Therefore, both Pareto and quasi-Pareto solutions should be evaluated more in-depth, before making a final decision for the heat pipe design. To do so, one of the clustering algorithms is employed for evaluating the solutions. An overview of the clustering algorithms can be found in Ref. [13,17,18]. If the potential solutions are systematically classified into several clusters, engineers can easily interpret the mathematical backgournd as well as engineering characteristics of the solutions in a more intuitive manner.

The clustering algorithm basically aims at minimizing the following clustering function:

$$C_F'(X,V,U) = \sum_{k=1}^{K}\sum_{i=1}^{n} u_{ik} \cdot dis(\vec{x}_i, \vec{v}_k) \quad (8)$$

Here, $X = \{\vec{x}_1, \ldots, \vec{x}_n\} \subseteq \mathbb{R}^d$ is a set of n solutions in d-dimensional space of real-value, where the n is number of solutions to be clustered. $V = \{\vec{v}_1, \ldots, \vec{v}_K\} \subseteq \mathbb{R}^d$ is a set of cluster centers, and K is the number of clusters. Also, $\vec{x}_i$ means the ith solution, $\vec{v}_k$ indicates the center of the k-th cluster, and $U = \{u_{11}, \ldots, u_{ik}, \ldots, u_{nK}\}$ is a set of clustering memberships. Finally, $u_{ik} \in \{0,1\}$ is the membership of $\vec{x}_i$ that belongs to the k-th cluster and $dis(\vec{x}_i, \vec{v}_k)$ presents the distance between $\vec{x}_i$ and $\vec{v}_k$.

4.1 Point symmetry distance measure

Many clustering algorithms adopt a Minkowski [17] metric to evaluate dissimilarity, i.e., the distance, $dis(\vec{x}_i, \vec{v}_k)$, in clustering functions. The Minkowski metric is defined as measuring the dissimilarity between the solution $\vec{x}_i = (x_{i1}, \cdots, x_{id})^T$ and the center of the cluster (search vector) $\vec{v}_k = (v_{k1}, \cdots, v_{kd})^T$:

$$d_{mink}(\vec{x}_i, \vec{v}_k) = [\sum_{j=1}^{d} | x_{ij} - v_{kj} |^r]^{1/r} \quad (9)$$

where $r \geq 1$. Three types of commonly used Minkowski metrics are illustrated in Fig. 7. The Euclidean distance ($r = 2$) is one of the most famous Minkowski distance metrics. Conventional clustering algorithms with the Euclidean distance tend to detect hyperspherical-shaped clusters.

The distribution shapes of Pareto and quasi-Pareto solutions are much closer to the combination of hyperellipsoidal or hyperline shape than that of the hyperspherical shape. Thus, the Euclidean distance measure may not be a good candidate for searching the characteristics of the solutions. For this reason, the point symmetry distance measure [19] is adopted.

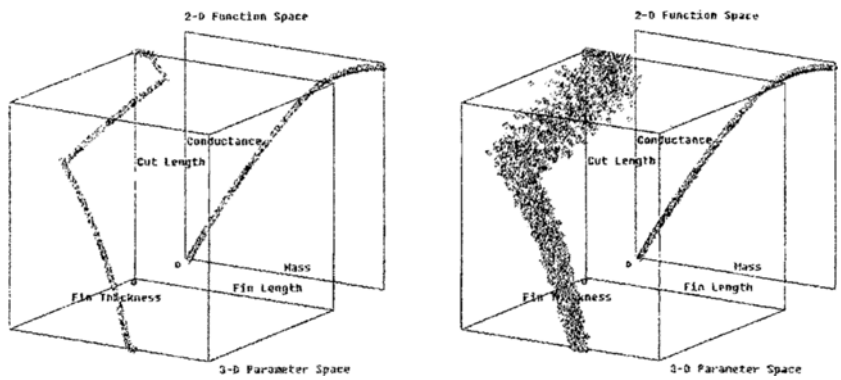

Fig. 6. Pareto (left) and quasi-Pareto (right) solutions of $\hat{\tilde{G}}_R$ and $\hat{\tilde{M}}_R$.

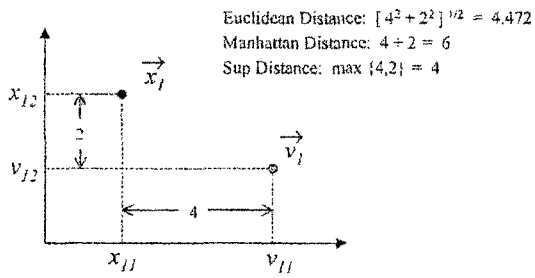

Fig. 7. Three common Minkowski metrics [17].

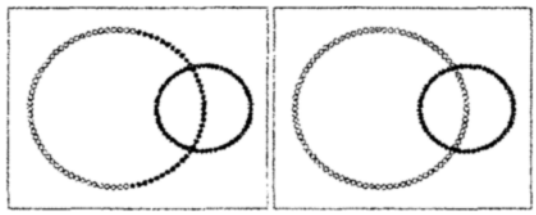

Fig. 8. Two clusters measured by using the Euclidean distance (left) and point symmetry distance (right).

The distance measure is more flexible for finding clusters of hyperellipsoidal or hyperline shapes. Given n solutions, the point symmetry distance between the solution $\vec{x}_i$ and the cluster center $\vec{v}_k$ is defined as:

$$d_{sym}(\vec{x}_i,\vec{v}_k) = min_{\substack{p=1,\ldots,n \\ and\ p\neq i}} \frac{\|(\vec{x}_i-\vec{v}_k)+(\vec{x}_p-\vec{v}_k)\|}{(\|(\vec{x}_i-\vec{v}_k)\|+\|(\vec{x}_p-\vec{v}_k)\|)} \tag{10}$$

where the denominator term normalizes the point symmetry distance. Due to normalization, the point symmetry distance becomes insensitive to the Euclidean distances $\|(\vec{x}_i-\vec{v}_k)\|$ and $\|(\vec{x}_p-\vec{v}_k)\|$.

Fig. 8 exhibits different clustering results of sample patterns, which were obtained from two different distance measures. The clustering result obtained from Euclidean distance shows that the two clusters are quantitatively well separated. The result obtained from point symmetry distance shows that each clustered pattern possesses the characteristics of its shape, i.e., a circle in this case. However, groups of patterns are often composed of patterns that have rare symmetric similarity among them. Therefore, Euclidean distance and point symmetry distance measure are flexibly used for the clustering function, Eq. (8). The flexible distance measure is defined as follows:

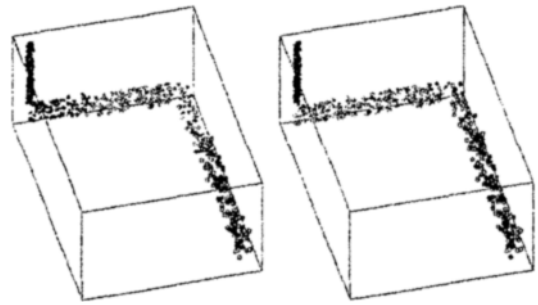

Fig. 9. Three clusters obtained by using the Euclidean distance (left) and point symmetry distance (right).

$$dis(\vec{x}_i,\vec{v}_k) = \begin{cases} if\ \ d_{sym}(\vec{x}_i,\vec{v}_k) < \theta, & d_{mink}(\vec{x}_i,\vec{v}_k),\ r=2 \\ else, & d_{sym}(\vec{x}_i,\vec{v}_k) \end{cases} \tag{11}$$

where θ is the trade-off parameter between two different distance measures. The results of the iterative clustering method such as the K-means algorithm [17,18] depend on the initial centers. In the proposed clustering function, the clustering result significantly changes as θ varies. To circumvent this probles, the flexible distance measure is adopted to the evolutionary clustering algorithm [12]. In minimizing the clustering function, the trade-off parameter is defined as a constant *a priori*. Only centers are considered as variables of the clustering function, and they are searched by evolutionary processes such as selection, recombination, and mutation.

Fig. 9 shows an example that verifies the proposed clustering algorithm. The patterns appearing in the figure are generated by imitating Pareto solutions. The result from Euclidean distance shows that three clusters are separated from each other only geometrically. However, the proposed flexible measure works well for clusters with linear structures. The result from the flexible distance measure demonstrates how the parametric characteristics is transformed in parameter space. It is confirmed by comparing both results in Fig. 9 that the proposed measure is better suited for extracting meaningful engineering information. Therefore, the proposed clustering is employed along with the flexible distance measure in the following section.

4.2 Cluster interpretation of pareto solutions

The proposed clustering method is applied to Pareto and quasi-Pareto solutions from Eqs. (6) and

(7). The solutions were clearly classified into two clusters that have distinct parametric characteristics. Cluster #1 includes the solutions mainly dominated by fin thickness and slightly dominated by cut length. The solutions in the cluster are not sensitive to fin length. The solutions in cluster #2 change as the fin length and the cut length vary. In this case, the thickness of the fin is fixed at its maximum value, 1.7mm.

Fig. 10 presents the clustering result in both function and parameter spaces. Since heat resistance decreases as fins become thicker, the solutions in cluster #1 with thicker fins have higher thermal conductance. However, in the case of cluster #2, whose solutions have long fins, the heat flux becomes smaller as the fin parts are located further from the pipe junction. Therefore, long fins simply increases the mass without improving conductance, which results in poor design. From this evaluation, heat pipe designers can clearly understand which combination of design parameters improves or deteriorates the quality of design by using the proposed visualization and clustering technique.

Fig. 11 shows the projection of parameter space onto the object function space. It is apparent from the figure that the solutions in cluster #1 are positively increasing both the thermal conductance and mass within a reasonable level. On the other hand, the solutions in cluster #2 are exponentially increasing the mass. For example, 63.6% increase in mass improves 84.8% of thermal conductance in cluster #1. However, in cluster #2, 46.9% increased mass enhances the conductance by only 25.6%. Thus, the solutions in cluster #1 can be better candidates for overall design in terms of mass minimization and conductance maximization. As shown in Fig. 11, *Point I* - the ideal point for DM - has the minimum mass and the maximum conductance. Therefore, *Solution A*, the closest solution from *Point I* can be one solution for DM. However, if the heat pipe designer emphasizes the maximization of thermal conductance more, given a relatively small mass, *Solution B* on the border between two clusters can be the most promising candidate for DM.

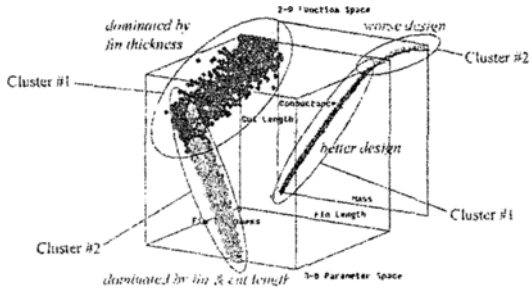

Fig. 10. Design parameters corresponding to optimum design.

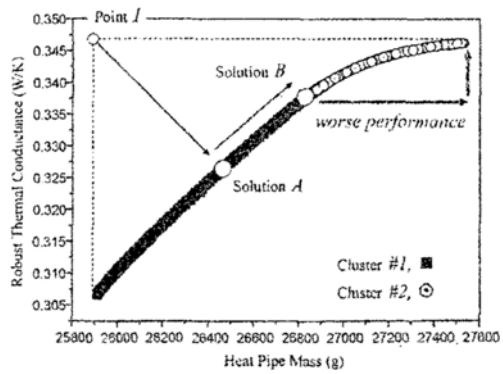

Fig. 11. Clustering in function space.

5. Conclusions

This research proposes a new methodology for analyzing Pareto and quasi-Pareto solutions in solving a multiobjective optimization problem. A synchronous 3D visualization technique explores the underlying characteristics of multidimensional solutions while illustrating the correlations among parameters, objective functions, and actual design parameters. Moreover, in clustering the potential solutions to find a meaningful decision for an engineering design, this paper presented a clustering algorithm, which incorpoates the hybrid distance measuring method for evaluating Euclidean and point symmetry distance. The clustering algorithm showed the similarity and dissimilarity among the solutions and provided illustrative information for designers. As a practical example, a design problem of a heat piping system in an artificial satellite was studied by the proposed approach. The multiobjective optimization problem involved two objective functions, two uncontrollable design parameters, and three parameters of the physical shapes of the heat pipes in the satellite. The synchronous 3D visualization helps designers to understand the global tradoffs of each particular design solution obtained from Pareto and quasi-Pareto solutions. Clustering the optimum and quasi-optimum solutions clearly guides the parameters of the physical shapes, which are directly tied to the quality of the design solution. With the help of the proposed 3D

visualization and clustering technique, the design engineer of a heat piping system in an artificial satellite can easily obtain useful information for finalizing the best design solution.

References

[1] R. V. Tappeta and J. E. Renaud, Iterative multiobjective optimization procedure, *AIAA Journa.*, 37 (7) (1999) 881-889.

[2] R. V. Tappeta and J. E. Renaud, Iterative multiobjective optimization design strategy for decision based design, *Journal of Mechanical Design.* 123 (2001) 205-215.

[3] Z. Meng and Y. H. Pao, Visualization and self-organization of multidimensional data through equalized orthogonal mapping, IEEE Transactions on Neural Network., 11(4) (2000) 1031-1038.

[4] J. Eddy and K. Lewis, Multidimensional design visualization in multiobjective optimization, 9th AIAA ISSMO Symposium on Multidisciplinary Analysis and Optimization (2002) 2002-5621.

[5] T. Kobayashi, T. Nomura, M. Kamifuji, A. Yao and T. Ogushi, Thermal robustness and mass optimization of heat pipe shape for spacecraft panel using a combination of responce surface methodology and monte carlo simulation, Proceedings of 28th Design Automation Conference, DETC2002/DAC-34055, (2002).

[6] W. Miller, Symmetry Groups and Their Applications, Academic Press, London, (1972).

[7] H. Weyl, Symmetry, Princeton University Press, Princeton, NJ, (1952).

[8] W. H. Kelly and J. H. Reisenweber, Thermal performance of embedded heat pipe spacecraft radiator panels, SAE Technical Paper, (1993) 932158.

[9] G. Taguchi, Design of Experiment, Japanese Standards Association(in Japanese), (1979).

[10] R. H. Myers and D. C. Montegomery, Response Surface Methodology: Process and Product Optimization Using Design Experiments, Wiley Inter-Science, (1995).

[11] G. Taguchi and S. Konishi, Orthogonal Arrays and Linear Graphs, ASI Press, Dearborn, MI, (1987).

[12] M. J. Jeong and S. Yoshimura, An evolutionary clustering approach to pareto solutions in multiobjective optimization, Proceedings of 28th Design Automation Conference, DETC2002/DAC-34048, (2002).

[13] M. J. Jeong, Integrated support system for decision-making in design optimization, PhD Thesis, The University of Tokyo, Tokyo, (2003).

[14] J. X. Chen, Data visualization: Parallel coordinates and dimension reduction, *Computing in Science and Engineering.* 3 (5) (2001) 110-113.

[15] A. Inselberg, Visulaiztion and data mining of high dimensional data, *Chemometrics and Intelligent Laboratory Systems*, 60 (2002) 147-159.

[16] H. Kawai, Development of a 3-d graphics and gui toolkit for making pre- and post-processing tools, Proceedings of the Conference on Computational Engineering and Science(in Japanese), 8 (2) (2003) 889-892.

[17] A. K. Jain and R. C. Dubes, Algorithms for Clustering Data, Prentice-Hall, Englewood, NJ (1989).

[18] B. Mirkin, *Mathematical Classification and Clustering,* Kluwer Academic Publishers, New York, NY, (1996).

[19] M. Su and C. Chou, A modified version of the k-means algorithm with a distance based on cluster symmety, IEEE Transactions on Pattern Analysis and Machine Intelligence, 23 (6) (2001) 674-680.

[20] T. Kashiwamura and M. Shiratori, Structural optimization using the design of experiments and mathematical programming, *Transactions of the JSME(in Japanese).* 62 (601) (1996) 208-223.